Electronic Supplementary Material (ESI) for Green Chemistry.

Supporting information

Extending the Chemical Product Tree: A Novel Value Chain for the Production of N-Vinyl-2-Pyrrolidones from Biogenic Acids

Moritz Otto Haus[a], Yannik Louven[a] and Regina Palkovits*[a]

[a]Institut für Technische und Makromolekulare Chemie (ITMC), RWTH Aachen University, Worringerweg 2, Aachen, DE-52074

*corresponding author: palkovits@itmc.rwth-aachen.de

Table of Contents

1. Reductive Amidation

2. Gas Phase Dehydration

1. Reductive Amidation

1.1 HPLC/GC Analysis and By-Products

The product spectrum of the reductive amidation of succinic acid with ethanolamine was analysed for different reaction times at harsh reaction conditions (200 °C, 150 bar H_2). The results of liquid phase analysis are displayed in **Figure S1** and respective data is given in **Table S1**. At short reaction times, the five components listed in the main reaction network (see main text) are sufficient to close the carbon balance with respect to the succinic acid educt, thus indicating good reaction selectivity. However, as the hydrogenation proceeds the contributions of these compounds decrease to below 80 mol.%. At the same time, several by-products such as butanols and N-ethyl-substituted compounds are evidenced by HPLC. Thus, the chemoselectivity of the Ru/C catalyst, which still allows for (i) the reduction of hydroxyl entities in the N-(2-hydroxyethyl)-substituent and (ii) the formation of pure reduction products is limiting to the overall yield of desired products.

For a more detailed analysis of the ongoing reactions the gas phase in the autoclave was also sampled. Analysis was conducted by GC (CO: 2 m Shin Carbon ST, 100/120 mesh packed column, ID = 1.00 mm; alkanes: 50m Plot Fused Silica, ID = 0.32 mm + DF = 5.0 µm) and MS (CIRRUS 2 by MKS Instruments, quadrupole detector) after the addition of acetylene as an internal standard. The results (**Table S1**) indicate a significant amount of methane in the gas phase, which likely originates from decarboxylation and subsequent methanation of the formed CO_2. Thus, C-C-bond cleavage presents a significant undesired reaction, which accounts for up to 16 mol.% of total conversion at high temperature and hydrogen pressure. Carbon dioxide itself was not evidenced, as may be expected at harsh reducing conditions. Lastly, small amounts of ethane are observed and might be attributed to the decomposition of ethanolamine. This may further be corroborated by the presence of small amounts of ammonia after a 24 h reaction. For shorter reaction times, NH_3 levels remain below the detection threshold due to the high dilution with remaining H_2 and possibly the good solubility of ammonia in the aqueous phase. Overall, neither ethane nor ammonia levels of the gas phase indicate an important contribution of ethanolamine decomposition.

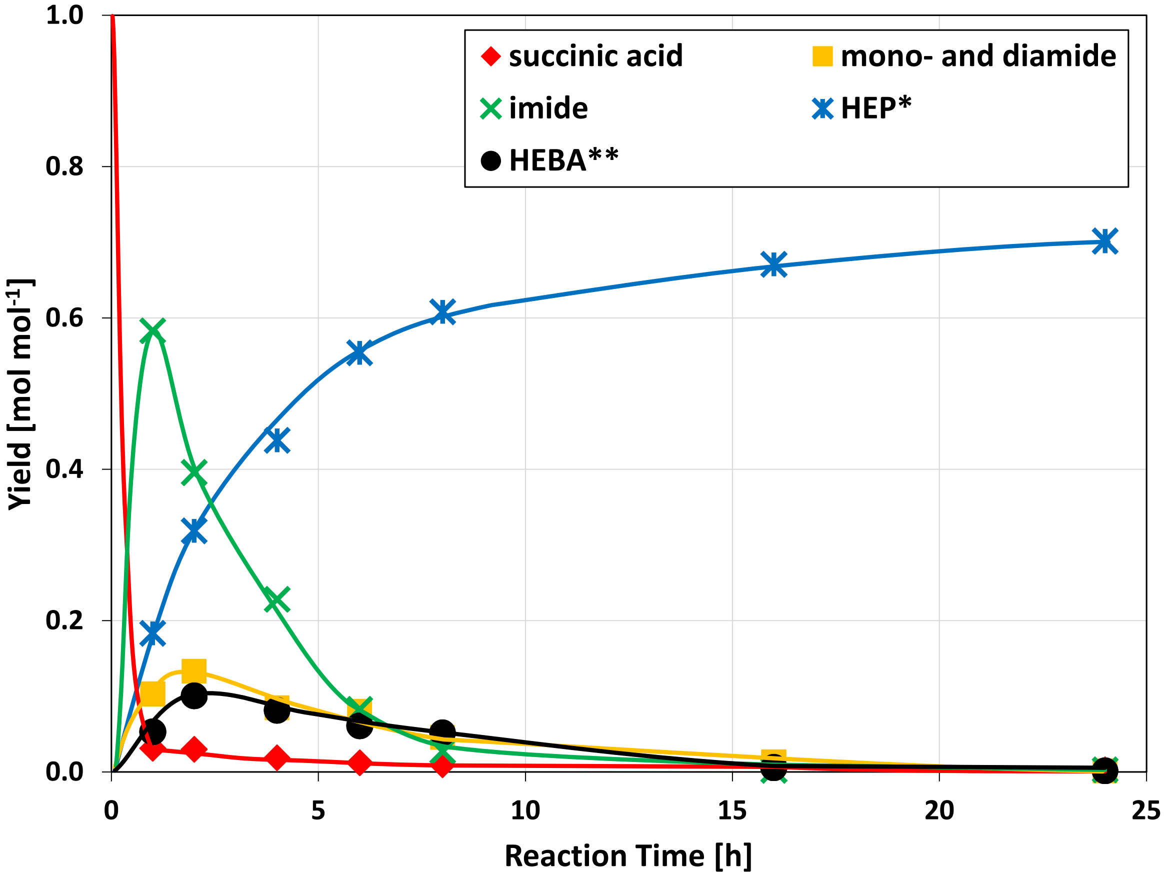

Figure S1: Concentration-time-profile of the reductive amidation of succinic acid with ethanolamine. (Cond.: 200 °C, 150 bar H_2, 750 rpm, 1.5 g acid, 1.5 g deionized water, 1 mol. equivalent of amine, 37.5 mg Ru/C) *HEP = N-(2-hydroxyethyl)-2-pyrrolidone, **HEBA = N-(2-hydroxyethyl)-4-hydroxybutanamide;

Table S1: Summary of liquid and gas phase analysis for the reductive amidation of succinic acid and ethanolamine. (Cond.: 200 °C, 150 bar H_2, 750 rpm, 1.5 g acid, 1.5 g deionized water, 1 mol. equivalent of amine, 37.5 mg Ru/C)

Reaction Time [h]	**1**	**2**	**4**	**6**	**8**	**18**	**24**
HPLC Yields [mol/mol$_{acid}$]							
succinic acid	0.03	0.03	0.02	0.01	0.01	0.01	0.00
mono- and diamide	0.10	0.13	0.09	0.08	0.05	0.01	0.00
imide	0.58	0.40	0.23	0.08	0.03	0.00	0.00
HEBA	0.05	0.10	0.08	0.06	0.05	0.01	0.00
HEP	0.18	0.32	0.44	0.55	0.61	0.67	0.70
ΣHPLC*	0.96	0.98	0.85	0.79	0.74	0.70	0.71
GC Yields [mol/mol$_{acid}$]							
methane	0.027	0.039	0.053	0.087	0.102	0.132	0.156
ethane	0.003	0.005	0.008	0.013	0.016	0.023	0.029
MS Yields [mol/mol$_{ethanolamine}$]							
ammonia**	0.00	0.00	0.00	0.00	0.00	0.00	0.02

*includes only the presented 5 components of the main reaction network.

**calculated from the 17 u mass fragment after accounting for the contribution of water vapor.

1.2 Absence of Mass Transfer Limitations

The absence of mass transfer limitations was asserted by testing for the influence of (i) stirring intensity and (ii) catalyst loading on the outcome of reductive amidation experiments. Experimental procedures and other parameters were as discussed in the main text.

The stirring speed was found to have negligible influence on the reaction outcome (**Figure S2** a). Minor variations in the determined yield and conversion levels for the displayed experiments are caused by the difficult quantification of HEBA (N-(2-hydroxyethyl)-4-hydroxybutanamide) *via* the chosen HPLC method. Since stirring intensity contributes to better mass transfer between the gas and liquid phases as well as between the bulk liquid and the catalyst grain, mass transfer limitations at these interfaces are unlikely. Further evidence is derived from a variation of catalyst loading, while keeping the product of the former with the reaction time constant. Under the assumption of a purely catalytic reaction, with a first order kinetics with respect to the catalyst, equal outcomes are expected for these experiments. Reduced yields, on the other hand, would indicate a suboptimal use of catalyst and thus likely mass transfer limitations. In reality, a slight increase in conversion together with a shift in product selectivity towards HEBA is observed (**Figure S2** b), which may be explained by (i) the contribution of non-catalytic equilibrium reactions between acid, amides and imide in the proposed reaction network and (ii) the thermally-activated condensation of HEBA to HEP. (i) leads to a reduction of N-(2-hydroxyethyl)succinimide concentration over the first 2-3 h of the discussed experiments, thus leading to a discrepancy in average substrate concentration for the hydrogenation in the presented experiments. The higher total yield for the 3h experiment follows straightforwardly, while the increased selectivity for HEBA is caused by the reduced time interval available for the occurrence of (ii).

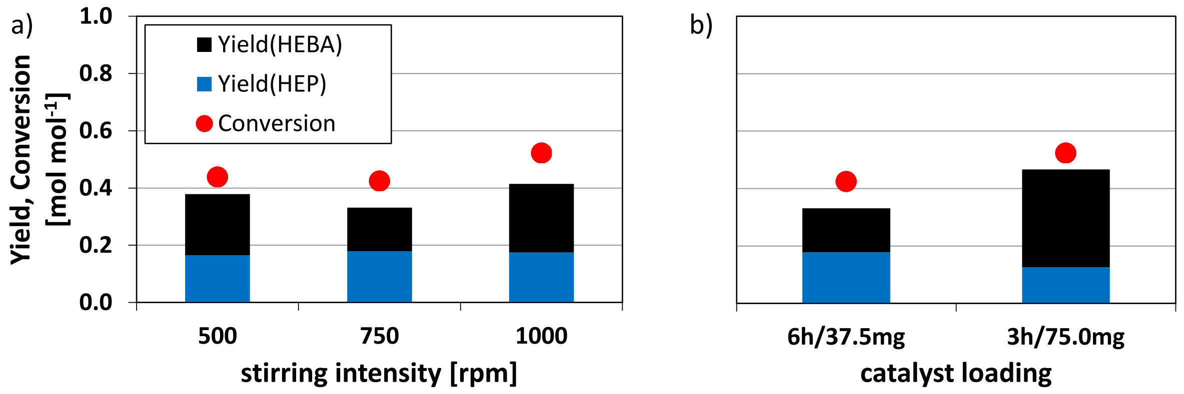

Figure S2: Influence of (a) stirring speed and (b) catalyst loading on the reduction of N-(2-hydroxyethyl)-succinimide. (Center point for all variations are standard conditions: 6 h, 750 rpm, 37.5 mg catalyst, 150 °C, 150 bar H_2 and ca. 2 g H_2O solvent)

1.3 Hot Filtration (Heterogeneous Nature of Catalyst)

Since Ru-leaching from the catalyst during the reaction could not be excluded, additional tests were performed to assert the heterogeneous nature of the commercial Ru/C catalyst. The reaction conditions were equivalent to those applied in catalyst recycling (200 °C, 150 bar H_2, 750 rpm, 50 mg catalyst). However, the hydrogenation was interrupted after 3 h as the autoclave was cooled to just below 100 °C. At this stage hydrogen was released from the autoclave, which was then opened to retrieve and filter the reaction mixture. Now free of carbon supported ruthenium, the reaction mixture was reinserted into the autoclave. After sealing, purging and raising $p(H_2)$ to 150 bar the autoclave was heated to 200 °C for another 3 h. As detailed in **Figure S3** neither the conversion, nor the sum of desired product yields shows a significant change after the catalyst was removed. A small increase in HEP concentration is caused by the non-catalytic cyclization of HEBA. The heterogeneous nature of Ru/C is therefore verified.

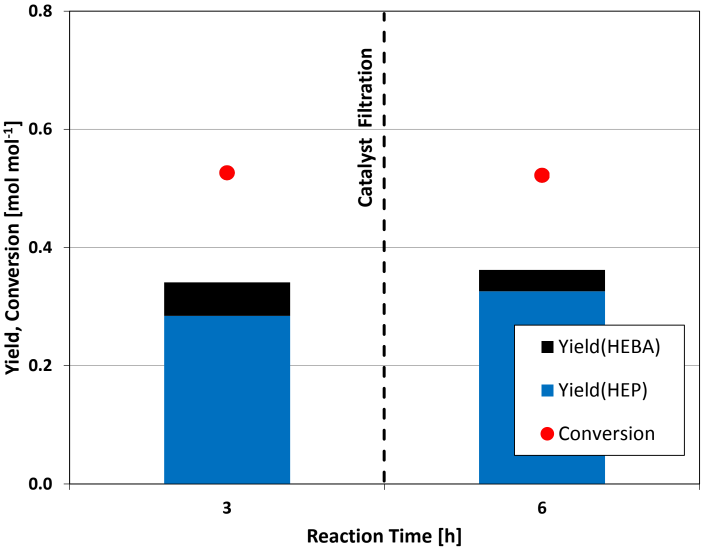

Figure S3: The effect of catalyst removal by filtration on an ongoing N-(2-hydroxyethyl)succinimide reduction experiment. (Cond: 200 °C, 150 bar H2, 750 rpm, 50 mg catalyst)

1.4 Catalyst Characterization

Methods

Different properties of the utilized catalysts were characterized by means of ICP-OES, N_2-physisorption, HAADF-STEM, CO-pulse chemisorption and FTIR spectroscopy of adsorbed pyridine. For ICP-OES measurements an aliquot of the reduced catalyst was dissolved in aqua regia using a microwave digestion vessel. The resulting clear liquid was diluted and measured on a SPECTROBLUE ICP-OES machine. N_2-physisorption was conducted on a QUADRASORB^{TM} SI (by Quantachrome) after degassing each sample at 200 °C in HV. BET surface areas were calculated from five adsorption points in the range $p/p_0 = 0.05\text{-}0.25$ (adsorption branch). TEM images were taken on a FEI Tecnai F20 operated in HAADF-STEM mode. For the determination of ruthenium particle size distributions, several hundreds of particles per catalyst were evaluated by application of the ImageJ software to the recordings. Several positions on the sample were included for the evaluation to guarantee statistical soundness of the obtained particle size data. For CO-pulse chemisorption, 60mg of dry and reduced sample was weighed into a quartz U-tube, functioning as fixed bed reactor. The filled tube was placed in a ChemBET Pulsar (Quantachrome), where potential passivation layers were removed from Ruthenium by a mild reduction at 200 °C (5 vol.% H_2 in Ar, 30 min). Next, hydrogen was removed by continuously flowing He at 350 °C for 1 h, before cooling down to room temperature and pulsing defined amounts of CO into the He flow. The amount of surplus CO was determined by means of a TCD located at the gas outlet. Dispersion values were calculated from the total amount of adsorbed CO and the metal content of the sample, assuming a stoichiometry of one molecule of carbon monoxide per surface metal atom. FT-IR spectra of adsorbed pyridine were recorded on a VERTEX70 spectrometer (Bruker). For this purpose, layered hybrid pellets of KBr and the studied material were formed on a hydraulic press. Firstly, 100 mg of KBr was pressed into a smooth, self-supporting wafer (10 mm diameter). Next, a second layer consisting of 20 mg of finely ground catalyst was pressed onto the first, granting a strong pellet with minimal interaction between KBr and the studied sample. The hybrid pellet was inserted into a home-made transmission cell and degassed *in situ* at 350 °C for 2 h while applying high vacuum (ca. 10^{-2} mbar). Next, the cell was cooled down to 80 °C for the recording of background spectra followed by saturation of the sample with gaseous pyridine sucked in from a reservoir. Excess and physisorbed pyridine was removed by the vacuum pump (1 h, 80 °C) before the final spectrum, used for the determination of acid sites, was taken. In accordance with earlier studies[1], the 1440-1465 cm^{-1} absorption band and the joint occurrence of bands at 1540, 1640 and 1485 cm^{-1} were taken as indicative of Lewis respectively Brønsted acid sites. An approximate quantification of these sites is based on the integrated molar extinction coefficients for the 1455 cm^{-1} band (2.22 cm μmol^{-1}) and the 1540 cm^{-1} band (1.67 cm μmol^{-1}) given by Emeis.[2]

Results

Due to its promising behaviour, commercial Ru/C was subjected to further characterization using the methods detailed above (**Table S2**). The results indicate a slight discrepancy between nominal and actual ruthenium loading. As a consequence, the ratio of noble metal to substrate used in our reactions is as low 0.1 mol.%, highlighting the activity of ruthenium for the challenging hydrogenation of imide carbonyls. This is at least partly due to the high surface area of activated carbon, which allows for good dispersion and thus utilization of the noble metal component.

This aspect was further analysed by HAADF-STEM. The recorded images show a uniform distribution of ruthenium particles (evidenced by EDX) on the carbon support (**Figure S4**). Evaluation of the images led to the particle size distribution displayed in **Figure S5**. Due to the low average particle size, ruthenium can be said to be well dispersed on the support material.

Table S2: Physical properties of the carbon-supported ruthenium catalyst (Ru/C).

Catalyst	BET Surface Area [$m^2\ g^{-1}$]	Pore Volume [ccm g^{-1}]	ICP-OES Metal Content [mg g^{-1}]
5wt.% Ru/C	858	0.69	33.1

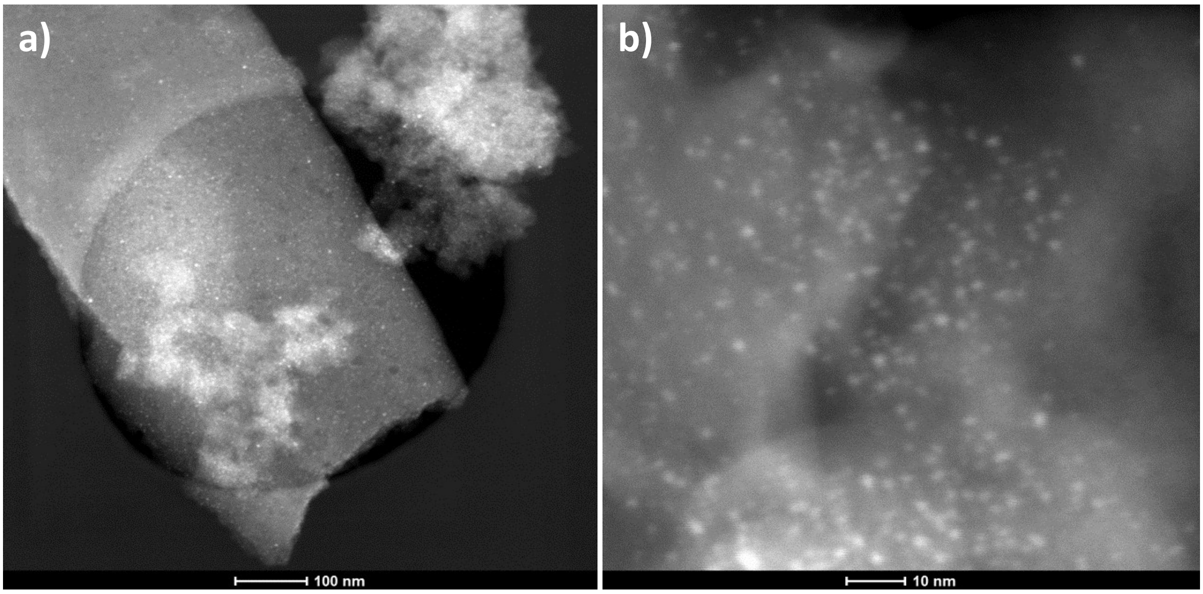

Figure S4: HAADF-STEM images of commercial Ru/C. Ruthenium particles (evidenced by EDX) are visible as bright dots. a) overview of a larger piece of the carbon support; b) one of the high magnification images used for particle size determination;

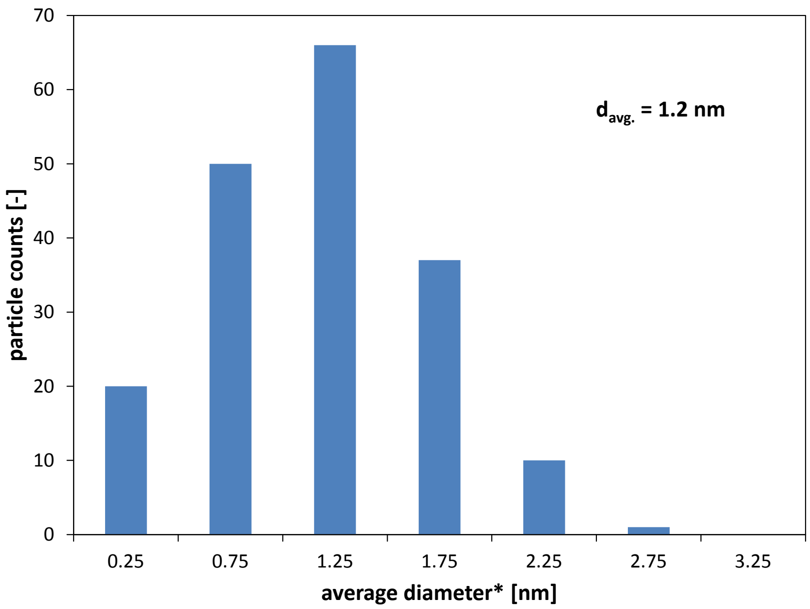

Figure S5: Ru particle size distribution of commercial Ru/C as determined from HAADF-STEM images; *individual particle size is calculated based on the assumption of (half-)spherical particles. $d_{avg.}$ is given on a number basis.

In order to identify the catalyst property mainly responsible for the activity difference between supported ruthenium catalysts, samples were analysed *via* CO-pulse titration and IR spectroscopy of adsorbed pyridine. The calculated values of metal dispersion decrease in the order Ru/C > Ru/TiO_2 ≈ Ru/ZrO_2 ≈ Ru/Al_2O_3 > Ru/SiO_2, thus providing an explanation for the lowered activity of ruthenium on a silica support. Here, the formation of large ruthenium particles might lead to a significant reduction of active surface atoms participating in reductive amidation. However, metal dispersion alone does not serve to explain activity differences between the remaining four catalysts. It would thus appear that acidity plays a role in the ongoing reduction of the C=O-bond, as has been shown for amide hydrogenation.[3] Results from FT-IR of adsorbed pyridine show that all of the tested oxide-supported catalysts show a significant amount of Lewis acid sites. However, the absolute numbers do not correlate with activity data from the main text. On the other hand, the two most active catalysts (Ru/ZrO_2 and Ru/Al_2O_3) both display a small amount of Brønsted acidity. Further research is required to clearly establish the respective correlation. In the meantime, the slightly higher dispersion of Ru/C as compared to oxide-supported analogues may indicate that improved dispersion of ruthenium somewhat mitigates the scarcity of acid sites on activated carbon with respect to overall catalyst activity.

Table S3: Physical properties of carbon-supported metal catalysts in this study.

Catalyst	Dispersion* [-]	Lewis Acidity** [µmol/g]	Brønsted Acidity** [µmol/g]
5wt.% Ru/C	0.16	n.d.	n.d.
5wt.% Ru/TiO_2	0.13	181	0
5wt.% Ru/ZrO_2	0.11	91	6
5wt.% Ru/Al_2O_3	0.11	269	13
5wt.% Ru/SiO_2	0.03	76	0

*determined by CO-pulse titration (stoichiometry Ru:CO = 1:1, based on nominal metal content); **determined by FT-IR studies of adsorbed pyridine at 80 °C;

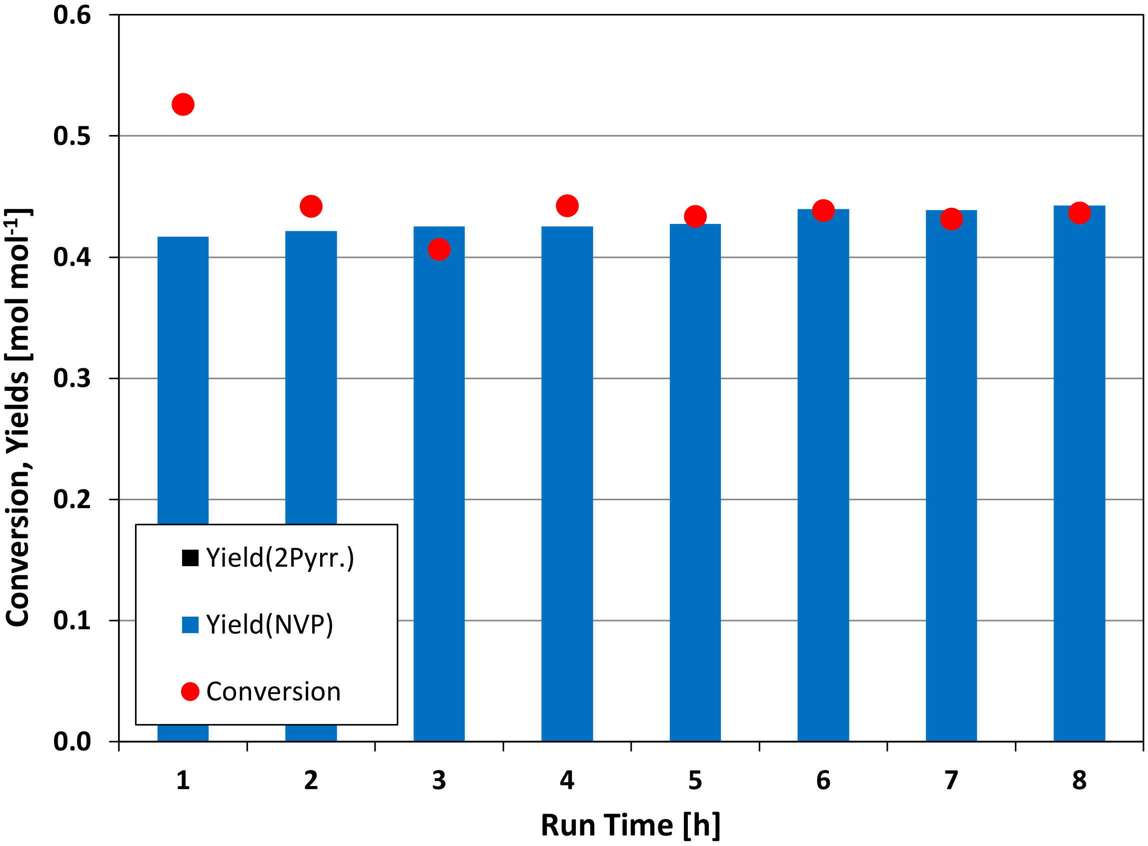

Figure S6: Results of the continuous gas phase dehydration of commercial N-(2-hydroxyethyl)-2-pyrrolidone over a NaO_2/SiO_2 (1:20) catalyst; (Products: NVP = N-vinyl-2-pyrrolidone, 2-Pyrr. = 2-pyrrolidone; Cond.: 0.1 g catalyst, 0.4 g SiC, 350 °C, 10 vol.% substrate, WHSV = 12 g_{HEP} $g_{catalyst}^{-1}$ h^{-1};)

2. Gas Phase Dehydration

2.1 Catalyst Stability

The stability of self-synthesized Na_2O/SiO_2 was tested during an 8 h dehydration experiment. Reaction conditions, most importantly WHSV, were chosen to limit conversion well below 100 %. As seen in **Figure S5**, NVP yield is stable over the entire runtime, thus indicating negligible deactivation.

After 8 h the substrate flow was stopped, and the catalyst dried using a steady nitrogen flow at reaction temperature for 1 h. Subsequently, sodium-doped silica was retrieved from the reactor and separated from SiC inert material by sieving. The extent of coking on the catalyst was evaluated by thermogravimetric analysis (TGA, Netzsch STA 409 with a 6.225.6-31 furnace type) in synthetic air. The main mass losses of the material were observed below 200 °C (9 wt.%) and between 400-500 °C (2 wt.%). While the former is attributed to water, which readsorbed to the spent catalyst, the latter presents evidence of arising coke deposits. However, coking accounts to an almost negligible amount of HEP conversion, which is in line with the observed catalyst stability.

2.2 Purification and Identification of Chemicals

Methods

^{1}H-NMR spectra were recorded on a Brucker Avance III (400 Hz) at room temperature. DMSO-d6 was used as NMR solvent.

Results

N-(2-hydroxyethyl)-3methyl-2-pyrrolidone was synthesized from 3-methyl-γ-butyrolactone (10 g) and ethanolamine (1 mol. equiv.) in sealed autoclaves containing an additional 10 g of deionized water as solvent. The reaction took place at 200 °C for 16 h in a stirred solution. Afterwards the desired product was obtained through distillation at reduced pressure (ca. 0.03 mbar, 110 °C top end). The ^{1}H-NMR spectrum of the purified pyrrolidone (**Figure S7**) is in line with expectations and shows excellent purity.

In between GC sample collection from the continuous gas phase dehydration the product stream was collected in a single vessel for the entire runtime of the experiment. Subsequently, the desired product (N-vinyl-3-methyl-2-pyrrolidone, 3MNVP) as well as the main by-product (3methyl-2-pyrrolidone) were purified by vacuum distillation (ca. 0.02 mbar). The light boiler (3MNVP) was collected first (ca. 35 °C top end), followed by 3methyl-2-pyrrolidone (ca. 80 °C). 1H-NMR spectra of the purified samples (**Figure S8** and **Figure S9**) are in line with expectations and show excellent purity.

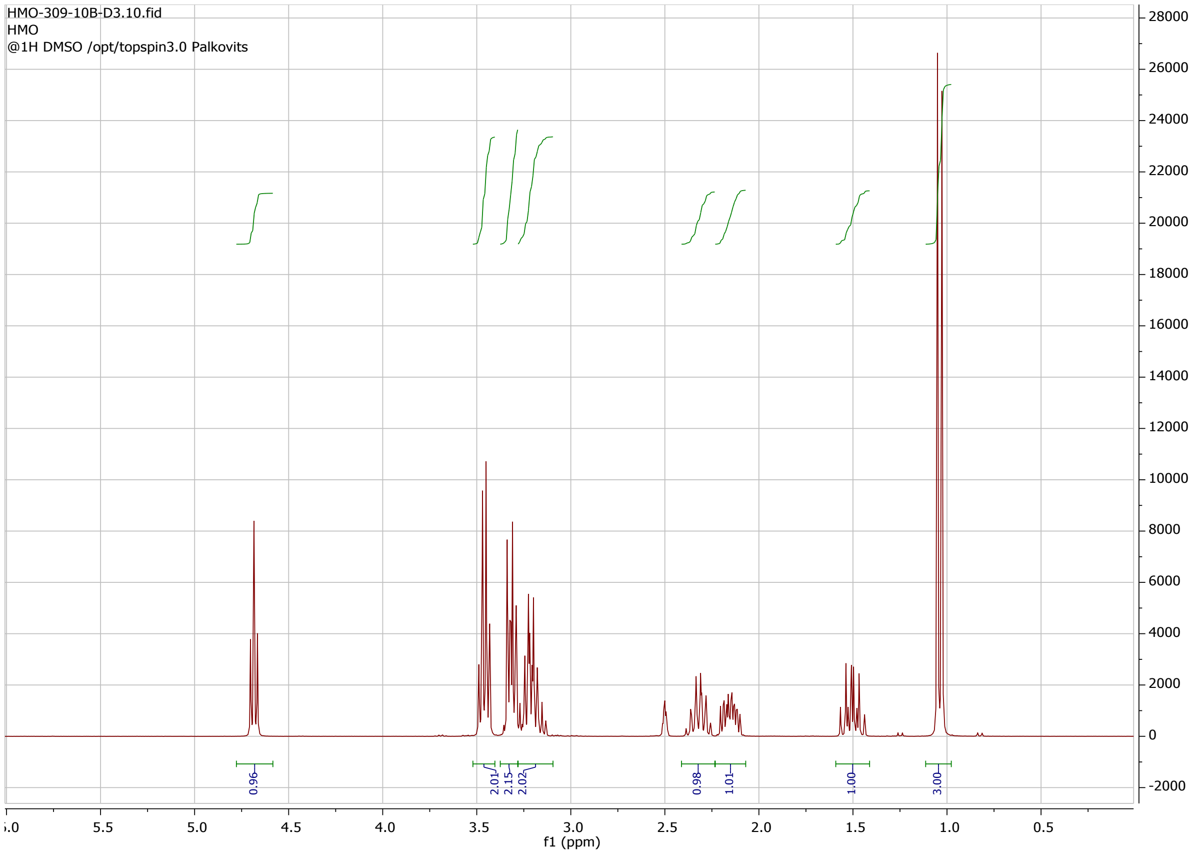

Figure S7: ^{1}H-NMR spectrum of self-synthesized N-(2-hydroxyethyl)-3methyl-2-pyrrolidone;

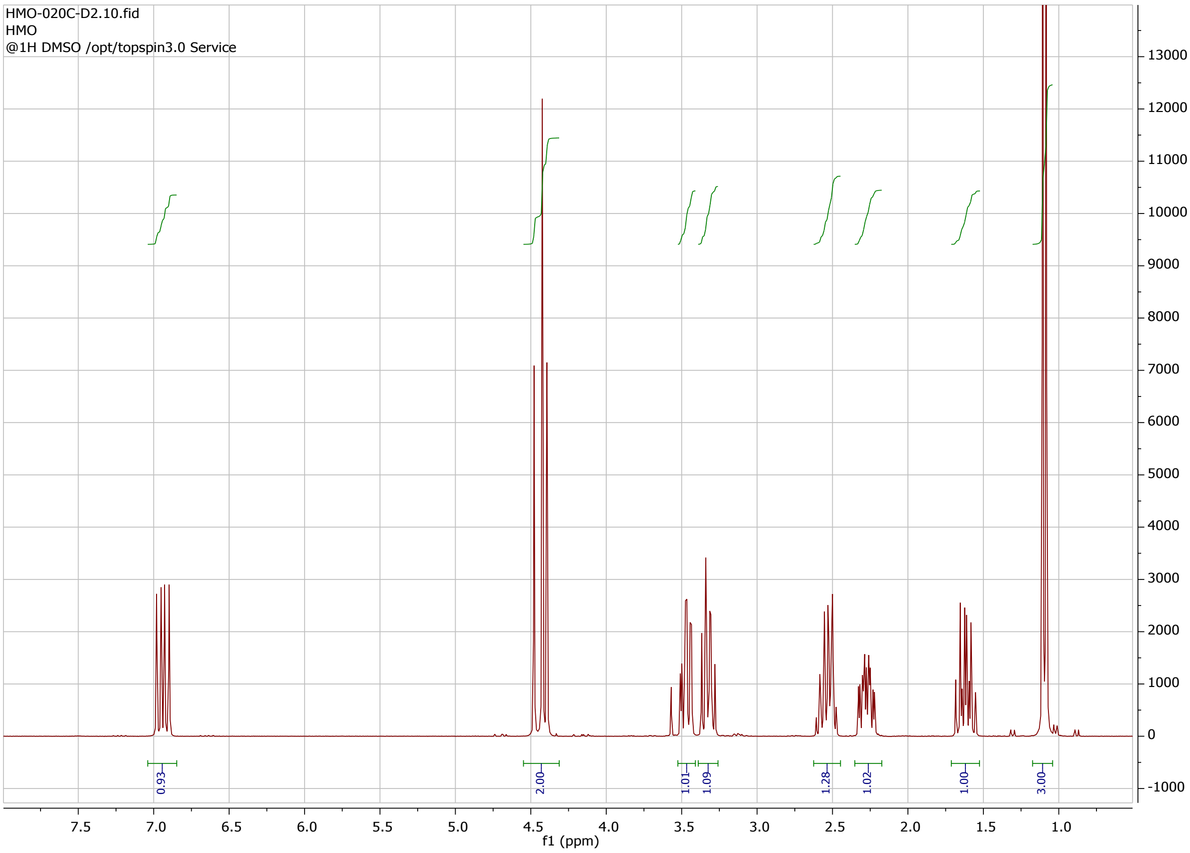

Figure S8: ^{1}H-NMR spectrum of N-vinyl-3-methyl-2-pyrrolidone from continuous gas phase dehydration;

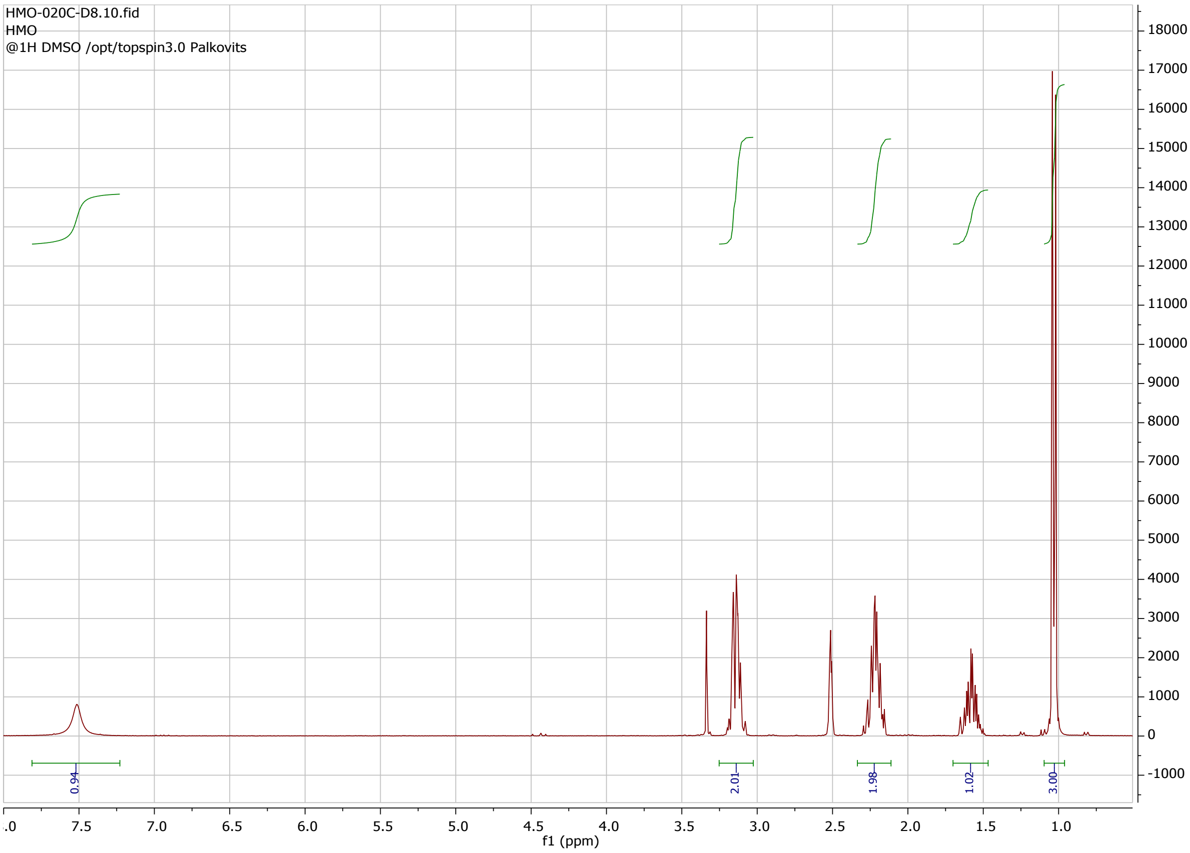

Figure S9: ^{1}H-NMR spectrum of 3methyl-2-pyrrolidone from continuous gas phase dehydration;

2.3 Gas Phase Dehydration of N-(2-Hydroxyethyl)-3methyl-2-pyrrolidone

The continuous gas phase dehydration setup was operated for 7 h with self-synthesized (see above) N-(2-Hydroxyethyl)-3methyl-2-pyrrolidone and NaO_2/SiO_2 (1:20) as catalyst. Samples were taken every hour and analysed *via* offline GC (**Figure S10**). Typically the carbon balance was within 100±5 mol.% as indicated by the comparison of yield and conversion values. A slight deactivation of the catalyst with time on stream is evident from a gradual increase of N-vinyl-3-methyl-2-pyrrolidone (=3MNVP) selectivity over the first 4h of operation. A subsequent increase in WHSV further decreases by-product quantities for the 6 and 7 h samples. After the end of the experiment the catalyst was removed from the reactor and displayed a slightly brown coloration (fresh catalyst = white) in line with coke formation.

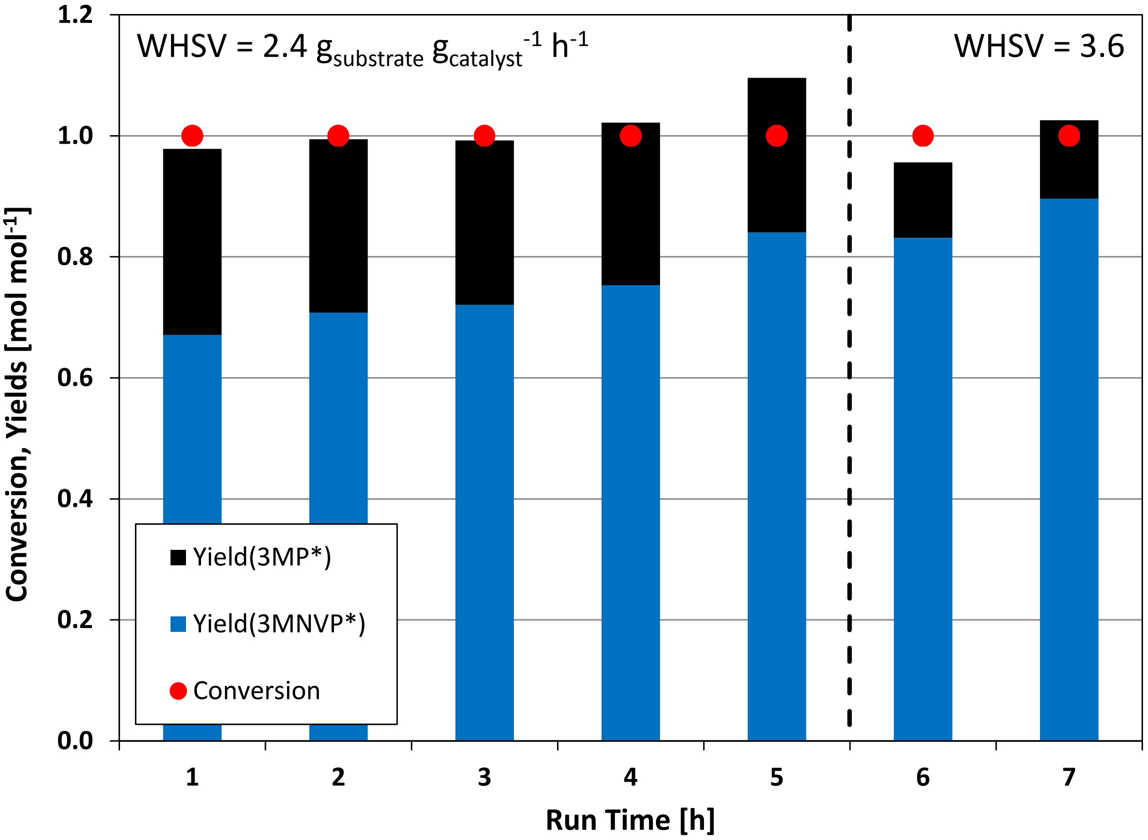

Figure S10: Results of the continuous gas phase dehydration of N-(2-hydroxyethyl)-3methyl-2-pyrrolidone over a NaO_2/SiO_2 (1:20) catalyst; (Cond: 1.0 g catalyst, 4.0 g SiC, 350 °C, 10 vol.% substrate, variable WHSV as indicated) *3MP = 3methyl-2-pyrrolidone; 3MNVP = N-vinyl-3-methyl-2-pyrrolidone;

Tabulated Values of Main Text Graphs

Table S4: Data corresponding to Figure 2 of the main text.

Reaction Time [h]	0.33	1	2	4	6	8	18	24
HPLC Yields [mol/mol_{acid}]								
succinic acid	0.75	0.33	0.23	0.09	0.07	0.06	0.03	0.02
mono- and diamide	0.17	0.14	0.12	0.09	0.10	0.11	0.12	0.10
imide	0.07	0.43	0.60	0.54	0.48	0.37	0.22	0.12
HEBA	0.00	0.01	0.03	0.06	0.08	0.12	0.15	0.17
HEP	0.00	0.03	0.06	0.13	0.19	0.23	0.35	0.40

Table S5: Data corresponding to Figure 4 of the main text.

Catalyst:	**Raney Ni**	**Ni/C**	**Co/C**	**Cu/C**	**Pd/C**	**Rh/C**	**Pt/C**	**Ru/C**
Yield(HEBA) [mol mol^{-1}]	0.01	0.00	0.00	0.00	0.00	0.00	0.00	0.15
Yield(HEP) [mol mol^{-1}]	0.02	0.00	0.00	0.00	0.01	0.04	0.04	0.18
Conversion [mol mol^{-1}]	0.08	0.00	0.00	0.06	0.07	0.09	0.06	0.47

Table S6: Data corresponding to Figure 5 of the main text.

	Reaction Temperature			**p(H_2)**			**m(H_2O)**		
Reaction Conditions:	**150 °C**	**175 °C**	**200 °C**	**50 bar**	**100 bar**	**150 bar**	**3.5 g**	**2 g**	**1.25 g**
Yield(HEBA) [mol mol^{-1}]	0.15	0.14	0.07	0.10	0.16	0.19	0.22	0.15	0.17
Yield(HEP) [mol mol^{-1}]	0.18	0.33	0.49	0.08	0.13	0.15	0.17	0.18	0.16
S(HEP+HEBA) [mol mol^{-1}]	0.78	0.77	0.67	0.73	0.77	0.81	0.75	0.78	0.70
Conversion [mol mol^{-1}]	0.43	0.61	0.84	0.24	0.37	0.42	0.52	0.43	0.48

Table S7: Data corresponding to Figure 6 of the main text.

Catalyst Use Cycle	**1**	**2**	**3**	**4**	**5**
Yield(HEBA) [mol mol^{-1}]	0.05	0.04	0.04	0.04	0.05
Yield(HEP) [mol mol^{-1}]	0.41	0.55	0.056	0.056	0.58
Conversion [mol mol^{-1}]	0.83	0.88	0.90	0.89	0.89

Tabulated Values of SI Graphs

Table S8: Data corresponding to Figure S2.

	stirring speed [rpm]			**reaction time/catalyst weight**	
Reaction Conditions	**500**	**750**	**1000**	**6h/37.5mg**	**3h/75.0mg**
Yield(HEBA) [mol mol^{-1}]	0.21	0.15	0.24	0.15	0.32
Yield(HEP) [mol mol^{-1}]	0.17	0.18	0.18	0.18	0.12

Conversion [mol mol^{-1}]	0.44	0.43	0.52	0.43	0.55

Table S9: Data corresponding to Figure S3. Catalyst was removed after 3 h.

Reaction Time [h]	**3**	**6**
Yield(HEBA) [mol mol^{-1}]	0.06	0.04
Yield(HEP) [mol mol^{-1}]	0.28	0.33
Conversion [mol mol^{-1}]	0.53	0.52

Table S10: Data corresponding to Figure S6.

Reaction Time [h]	**1**	**2**	**3**	**4**	**5**	**6**	**7**	**8**
Yield(NVP)	0.42	0.42	0.43	0.43	0.43	0.44	0.44	0.44
Yield(2-Pyrr.)	0.00	0.00	0.00	0.00	0.00	0.00	0.00	0.00
Conversion	0.53*	0.44	0.41	0.44	0.43	0.44	0.43	0.44

Table S11: Data corresponding to Figure S10.

Reaction Time [h]	**1**	**2**	**3**	**4**	**5**	**6**	**7**
WHSV [$g_{substrate}$ g_{cat}^{-1} h^{-1}]	**2.4**					**3.6**	
Yield(3MNVP)	0.67	0.71	0.72	0.75	0.84	0.83	0.90
Yield(3MP)	0.31	0.29	0.27	0.27	0.26	0.12	0.13
Conversion	1.00	1.00	1.00	1.00	1.00	1.00	1.00

Literature

1 E.P. Parry, *Journal of Catalysis*, 1963, **2**, 371-379.
2 C.A. Emeis, *Journal of Catalysis*, 1993, **141**, 347-354.
3 K. Shimizu, W: Onodera, A.S. Touchy, S.M.A.H. Siddiki, T. Toyao and K. Kon, *ChemistrySelect*, 2016, 4, 736-740.